

Figure 22 Average snow temperature profiles for the cold (Julian days 107, 111, 113) and warm (Julian days 164, 168, 169) conditions during the SIMMS'92 spring program (Barber et al. 1995), Copyright by AGU).

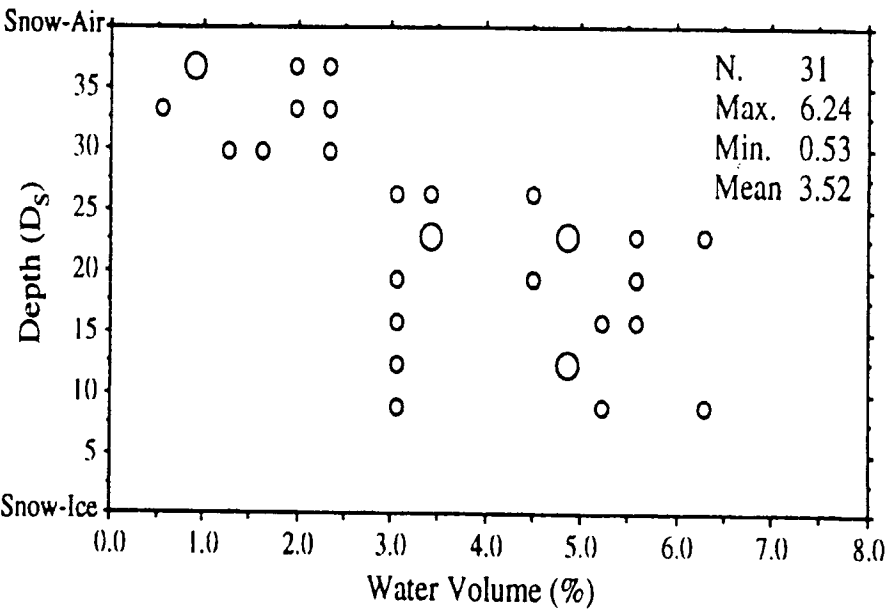


Figure 23 Snow wetness (percent liquid water by volume), as a function of depth, from Julian days 164, 168, and 169. Larger symbols denote overlapping data points (Barber et al. 1995, Copyright by AGU).

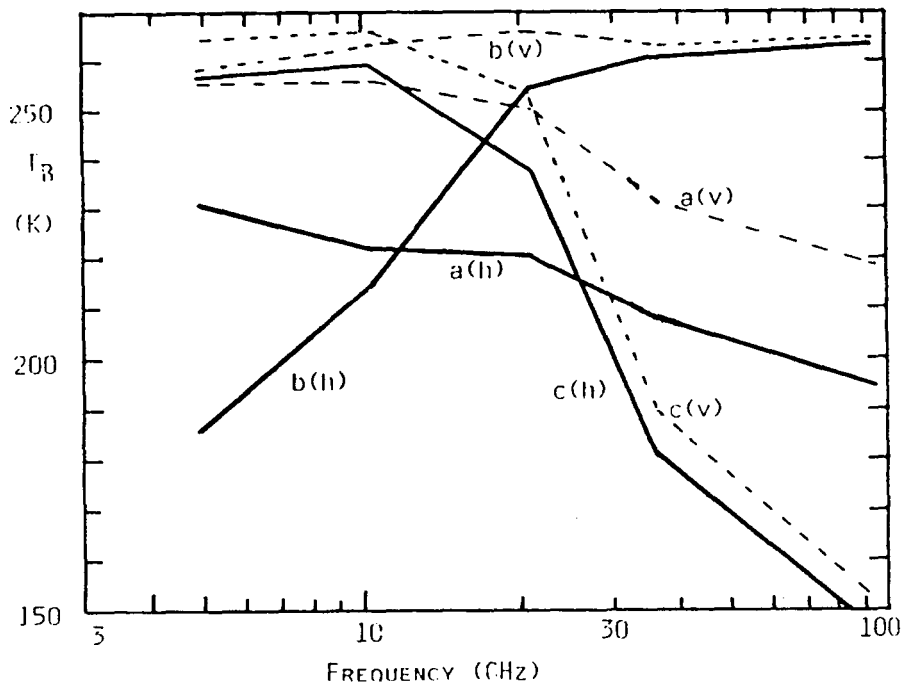


Figure 24 Average spectra of brightness temperatures observed at horizontal and vertical polarization and at 50° nadir angle. (a) During high winter condition, snow depths of all measurements normalized to 48 cm water equivalent, (b) wet firn layer of at least several centimetres on the surface of the snow cover, (c) thick (at least several centimetres) crust of refrozen firn (Schanda et al. 1983, with permission of Tayler and Francis).

Note that these idealized scetches are based on physical measurement, but do not represent distinct measurement. Ice lenses as depicted in Figure 25 may vary in number and density. But if they are present, they are found on nearly all floes within an area comparable to several SSM/I footprints. Large variations in the occurrence of ice lenses have been observed from year to year. Figures 27 and 28 illustrate the influence of distinct parameters on the brightness temperature, allowing to assess the correctness of the snow part of the sea ice module. In Figure 27 the change of the emitted radiation of an originally bare ice floe by an increasing snow layer has been observed. Garrity explains the rather quick and large response of the brightness temperature with the onset of snowfall by the small amount of free water (0.5 %) within the new snow, which increases the absorption by, and therefore the emission from, the snow. Figure 28 shows the change of the emissivity with snow wetness, compiled from several different sources.

This information is further condensed in the idealized scetch Figure 29. Finally, Figure 30 attempts to conclude the influence of different snow cover types on the brightness temperature. The vertical polarized brightness temperature is always greater for first-year and multiyear ice during the onset of melt than it is when the snow is dry.

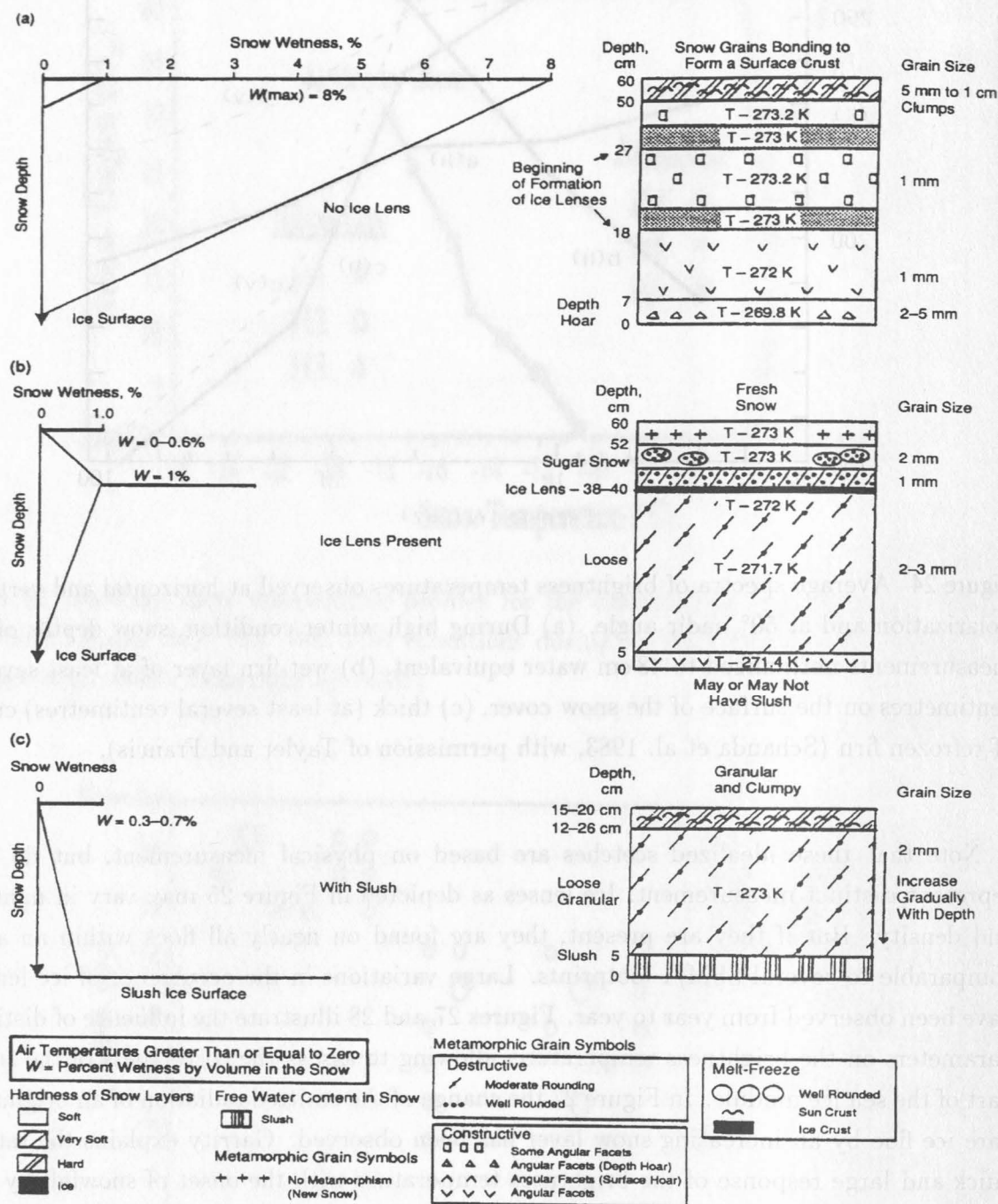


Figure 25 Snow models for spring in the Arctic for: (a) early spring, when a snow cover with no ice lenses is present; (b) mid-spring, when ice lenses are present in the snow cover; and (c) late spring, when slush is present at the snow-ice interface (Garritty 1992, Copyright by AGU).

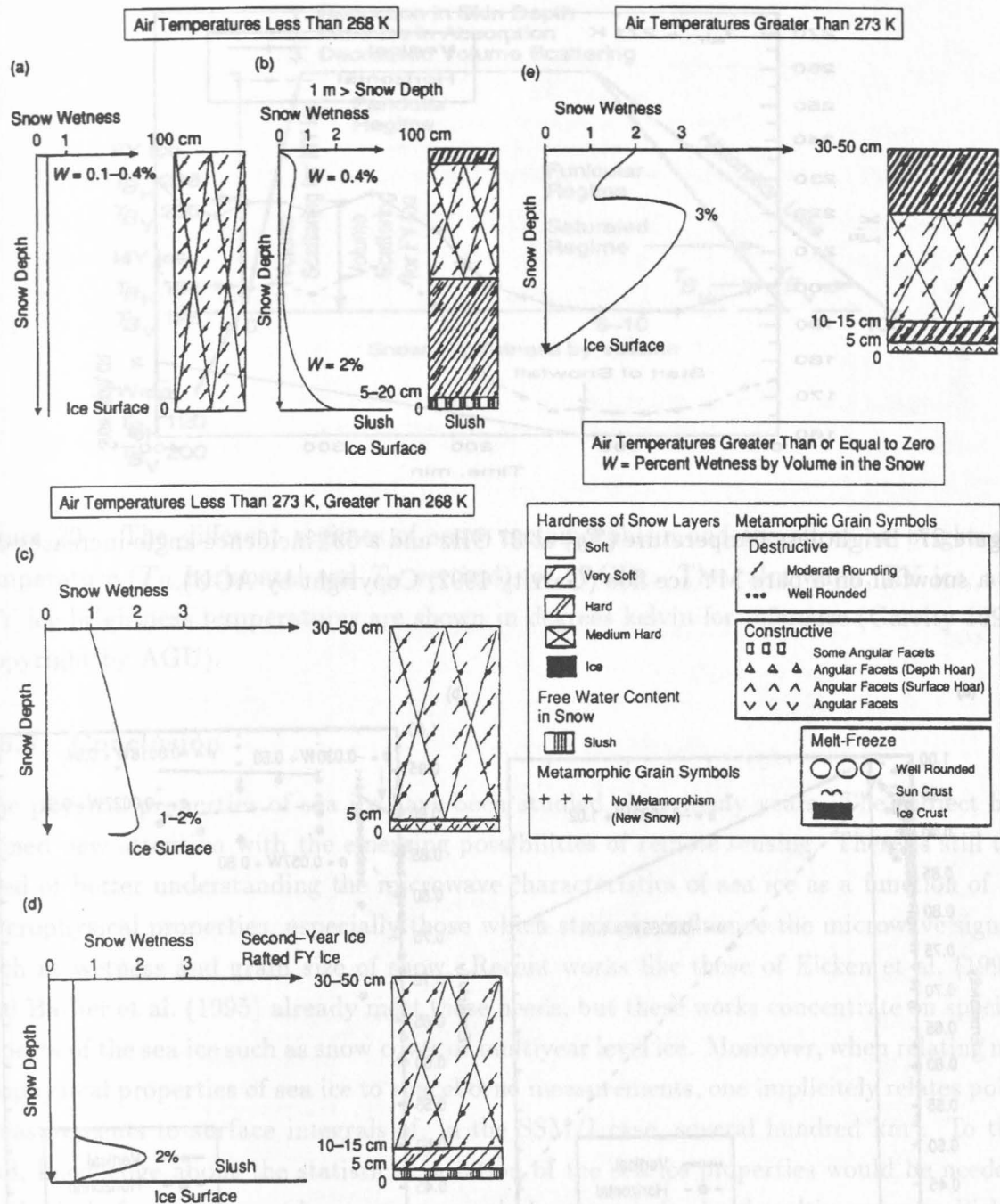


Figure 26 Snow models for spring in the Weddell Sea, Antarctic, are shown for air temperatures less than 268K (a) without and (b) with slush at the snow–ice interface. The same features are shown for an air temperature between (c) 268 and (d) 273 K. The snow wetness distribution changes significantly when (e) the air temperature is greater than 273 K. (a), (b), (c) and (d) are representative snow covers found at the western Weddell Sea ice edge; (d) and (e) are found at the eastern ice edge. (e) is also characteristic of the interior of the Weddell Sea. There is no descriptive snow model close to Antarctica presented (Garrity 1992, Copyright by AGU).

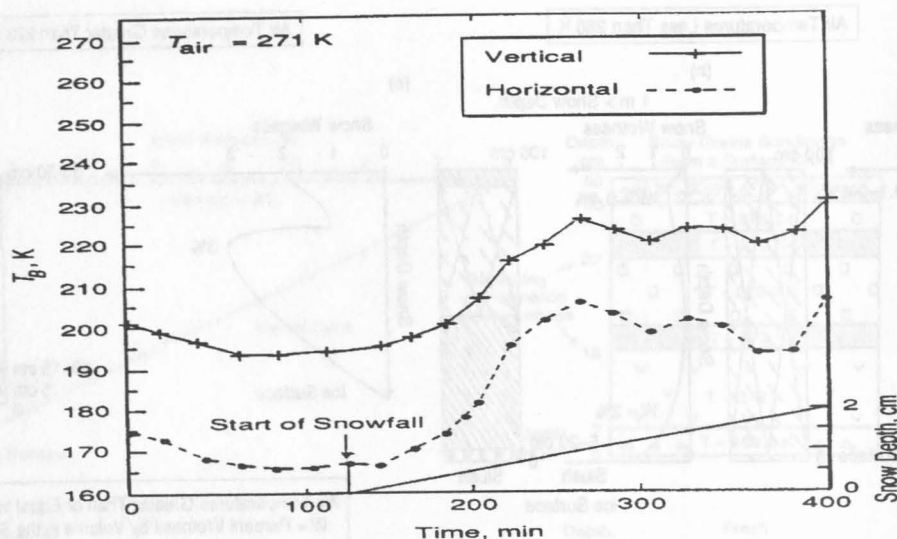


Figure 27 Brightness temperature (T_B) at 37 GHz and a 53° incidence angle increases due to a snowfall on a bare MY ice floe (Garrity 1992, Copyright by AGU).

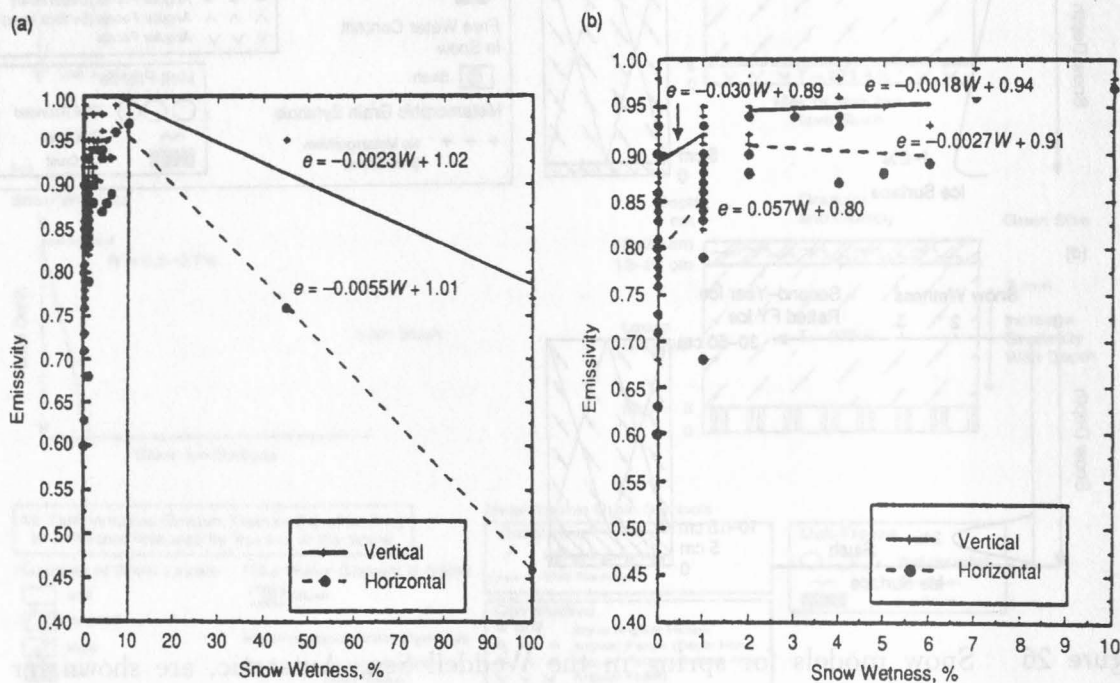


Figure 28 (a) Composite of snow wetness measurements, expressed as a percent of free water by volume, combined with satellite, groundbased, and ship-based radiometric measurements at 37 GHz and a 53° incidence angle. The measurements are from snow-covered floating ice. The scatter in emissivity near 0% wetness is mainly due to the different ice types present. (b) An enlargement of the right half of (a) shows more detail (Garrity 1992, Copyright by AGU).

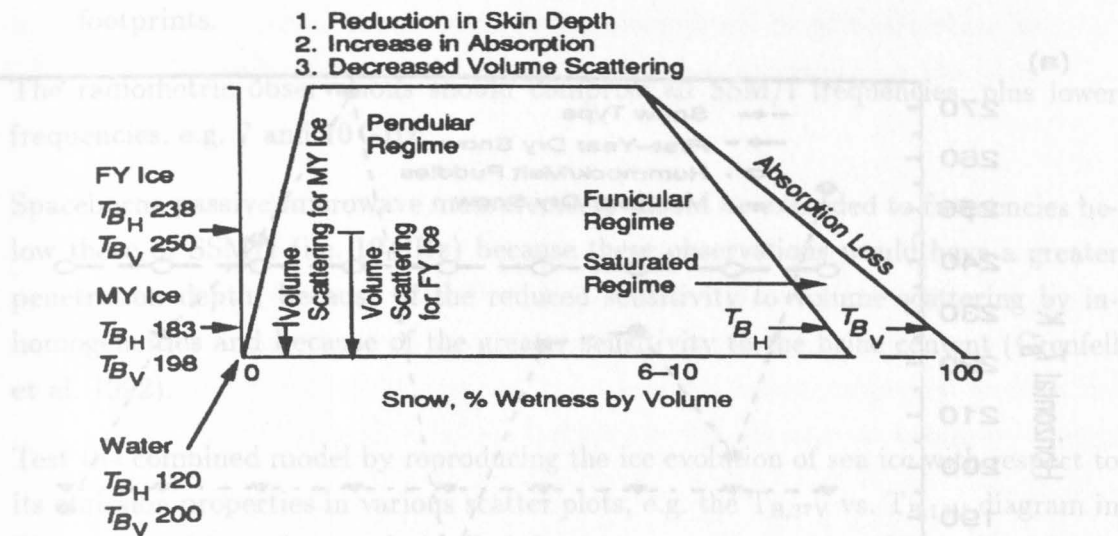


Figure 29 The different regimes of snow metamorphism and the effect on brightness temperature (T_B horizontal and T_B vertical) for 37 GHz. The calm water, FY ice, and MY ice brightness temperatures are shown in degrees kelvin for reference (Garrity 1992, Copyright by AGU).

2.6.5 Conclusion

The physical properties of sea ice have been studied since many years. The subject has gained new attention with the emerging possibilities of remote sensing. There is still the need of better understanding the microwave characteristics of sea ice as a function of its microphysical properties, especially those which strongly influence the microwave signal, such at wetness and grain size of snow. Recent works like those of Eicken et al. (1995) and Barber et al. (1995) already meet these needs, but these works concentrate on specific aspects of the sea ice such as snow cover or multiyear level ice. Moreover, when relating microphysical properties of sea ice to spaceborne measurements, one implicitly relates point measurements to surface integrals of, in the SSM/I case, several hundred km². To this end, knowledge about the statistical variation of the sea ice properties would be needed. Such kind of measurement has up to now only been made for level multiyear ice by Eicken et al. (1995). For other ice types, these properties are unknown.

The following investigations are recommended for further research:

- Simultaneous microphysical and radiometric measurements of sea ice. Emphasis should be put
 - on complete observations of all parameters listed in Table 2, eventually modified according to the results of the sensitivity analysis and

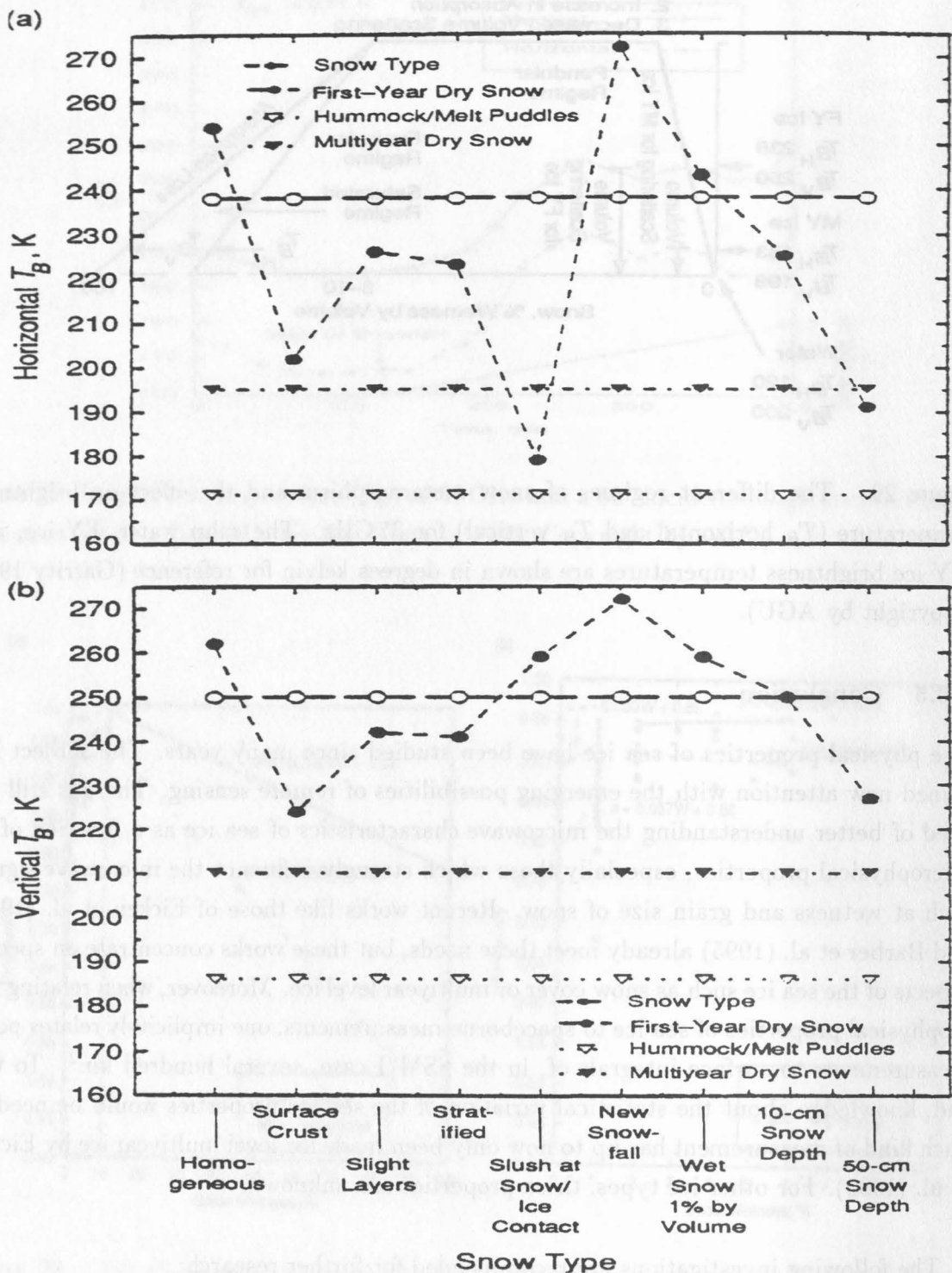


Figure 30 Influence of snow on brightness temperature at a frequency of 37 GHz and an incidence angle of 53° for (a) horizontal and (b) vertical polarizations (Garrity 1992, Copyright by AGU).

- on the statistical variation of the parameters at scales of spaceborne radiometer footprints.

The radiometric observations should comprise all SSM/I frequencies, plus lower frequencies, e.g. 7 and 10 GHz.

- Spaceborne passive microwave measurements should be extended to frequencies below those of SSM/I (i.e. 19 GHz) because these observations would have a greater penetration depth, because of the reduced sensitivity to volume scattering by inhomogeneities and because of the greater sensitivity to the brine content (Grenfell et al. 1992).
- Test the combined model by reproducing the ice evolution of sea ice with respect to its emission properties in various scatter plots, e.g. the $T_{B,37V}$ vs. $T_{B,18V}$ diagram in Figure 31, with preference for well-defined ice scenarios, e.g. multiyear level ice in the sense of Figures 11 and 12.

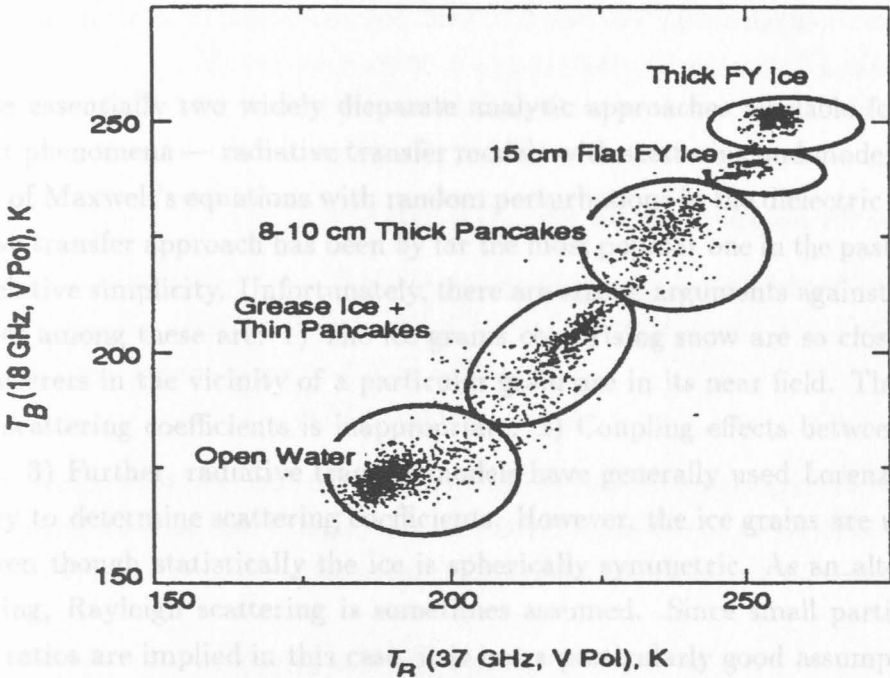


Figure 31 Cluster observations of some thin ice types and first-year ice from MIZEX'87 in the northern Greenland Sea. V-pol observations are at a nadir angle of 50°(Grenfell et al. 1992, Copyright by AGU).

- The inner coupling of the ice parameters with the ice ageing is not well understood and should be investigated as well in field studies as in models. Especially about the parameters brine pocket size and frequency, snow cover, surface roughness, ice thickness change together as ice ages (Grenfell et al. 1992).

- The ability of discriminating further ice types, e.g. thin ice, would help to a better understanding of ice dynamics and mass balance. Especially the potential of multisensor analyses should be considered (Grenfell et al. 1992, Hunewinkel 1996).

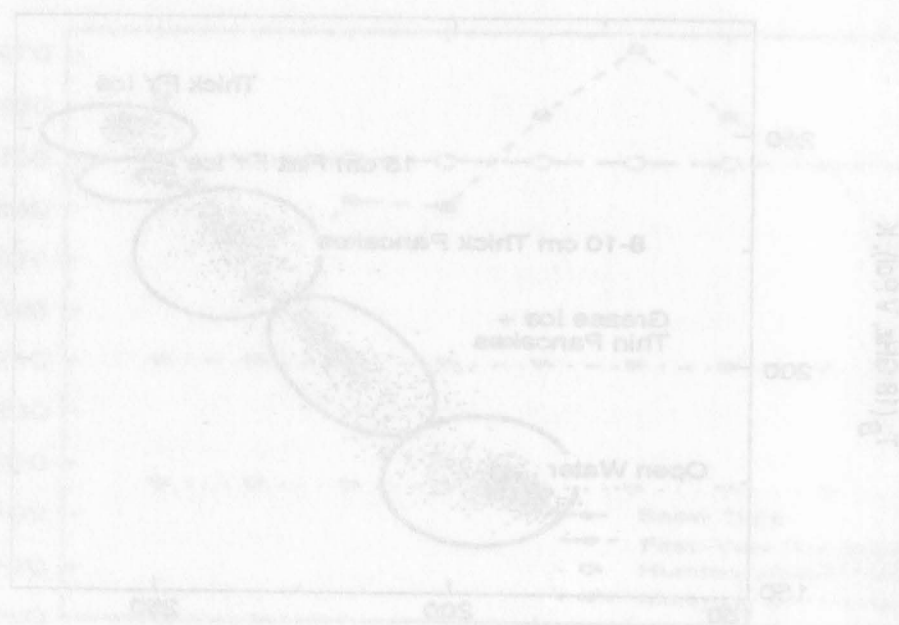


Figure 31: Cluster observations of four ice types and first-year ice from MEX-87 in the northern Greenland Sea. V-pol observations are at a nadir angle of 50° (Grenfell et al. 1992. Copyright by AGU).

- The roughness of the ice parameters with the ice surface is a well known problem and should be investigated as well in field studies as in models. Especially roughness of the parameters have pocket size and frequency, snow cover, surface roughness, ice thickness change, together as ice ages (Grenfell et al. 1992).

3 Combined Model

3.1 Sea-ice Module

3.1.1 Introduction

Sea Ice is a complex substance of considerable importance for the regional polar and global climate and there are many attempts to detect it with remote sensing methods. An essential ingredient of any attempt to achieve a quantitative understanding of the microwave radiometric and radar signatures of the diverse types of naturally occurring sea ice is a knowledge of the dielectric properties of the ice. A summary of experimental work on the dielectric constant involving both artificial and natural sea ice may be found by Vant et al. (1978).

A possible snow cover on sea ice may strongly influence the microwave brightness temperature of sea ice. It is generally accepted that the principal physical cause of the observed brightness temperature behaviour of snow is scattering from its constituent ice grains.

There are essentially two widely disparate analytic approaches available for studying the resultant phenomena — radiative transfer models with scattering and models based on the solution of Maxwell's equations with random perturbations in the dielectric properties. The radiative transfer approach has been by far the most popular one in the past, no doubt due to its relative simplicity. Unfortunately, there are strong arguments against its applicability. Chief among these are: 1) The ice grains comprising snow are so closely packed that the scatterers in the vicinity of a particular grain are in its near field. Thus, the use of far field scattering coefficients is inappropriate. 2) Coupling effects between particles are ignored. 3) Further, radiative transfer models have generally used Lorenz-Mie scattering theory to determine scattering coefficients. However, the ice grains are usually not spherical even though statistically the ice is spherically symmetric. As an alternative to Mie scattering, Rayleigh scattering is sometimes assumed. Since small particle size to wavelength ratios are implied in this case, it is not a particularly good assumption above 30 GHz. Whether or not one is inclined to ignore these difficulties, it is undeniable that radiative transfer theories for example have led to predictions of unacceptably low brightness temperatures for dry snow at sufficiently high frequencies (Stogryn 1986). For these reasons, it is desirable to investigate alternatives to radiative transfer models.

Among the approaches not based on radiative transfer the strong fluctuation theory is among those which have led to the best results when trying to reproduce experimental parameters of sea ice signatures.

The model of Stogryn (1987) in the implementation of Grenfell describes the emissivity of an isothermal sea ice layer in the microwave region between 1 and 100 GHz. It is based on the many-layer-strong-fluctuation-theory, a self-consistent theory relying on the Maxwell equations. The sea ice consists (in view of the model) of isothermal layers of snow and ice. For each of them different parameters are defined to describe its structure and constituents. The layer structure is used to calculate the dielectric properties and the emissivity of the sea ice. The calculation of the brightness temperature of sea ice is described in section 3.1.1.1. Under the layers of the ice the model needs an optically thick layer — normally water — or thick ice.

In the next section, we describe the strong fluctuation theory. Then we explain the layer structure with the sea-ice-, snow- and water-layers and their implementation into the model. Furthermore we will give some typical values for the different parameters. The last section presents some results.

3.1.1.1 Some Details of the Many Layer Strong-Fluctuation-Theory In the strong fluctuation theory the electric field is \vec{E} decomposed into two components, one for the mean field \vec{E}^m and one for the randomly fluctuating part \vec{E}^r :

$$\vec{E} = \vec{E}^m + \vec{E}^r. \quad (27)$$

From Maxwell's equations we get for the electric field \vec{E}

$$\nabla \times \nabla \times \vec{E} - k_0^2 K_0 \vec{E} = -\Delta L \cdot \vec{E} \quad (28)$$

with

$$\Delta L = -k_0^2 (K_0 - K^r). \quad (29)$$

The term on the right hand side of (28) accounts for the effects of scattering due to random inhomogenities (K_0 is the average dielectric constant, K^r the random dielectric constant and $k_0 = \omega/c$). For the mean and fluctuating part we get, respectively

$$\nabla \times \nabla \times \vec{E}^m - k_0^2 K_0 \vec{E}^m = \langle \Delta L \cdot \vec{E} \rangle, \quad (30)$$

$$\nabla \times \nabla \times \vec{E}^r - k_0^2 K_0 \vec{E}^r = -(\Delta L \cdot \vec{E} - \langle \Delta L \cdot \vec{E} \rangle). \quad (31)$$

The bilocal approximation (Stogryn 1983a) yields from equations (30) and (31) by ignoring terms of

$$\xi := \Delta L (I + S \Delta L)^{-1}, \quad (32)$$

the random tensor describing the fluctuating part of the dielectric constant, of higher order than two (Stogryn, 1983a) and using the tensor operator $L_0 = \nabla \times \nabla \times - k_0^2 K_0$

$$(L_0 - \langle \xi G \xi \rangle) \vec{E}^m = 0 \quad (33)$$

and

$$L_0 \vec{E}^r = -\xi \vec{E}^m. \quad (34)$$

For the explanation of G see (40). The assumption for the approximation used in (33) and (34) is

$$\left| \frac{\langle (K^r)^2 \rangle}{K_0^2} K_0 k^2 l^2 \right| \ll 1 \quad (35)$$

with l as the scale of the inhomogeneities.

I in (32) is a unit dyad, the coefficient S of the delta function in (39) is part of the Green's function Γ which satisfies the differential equation

$$\nabla \times \nabla \times \Gamma - k_0^2 K_0 \Gamma = \delta(r - r') \quad (36)$$

for the problem without random fluctuations. In general S is a tensor. For brine pockets in sea ice the model uses ellipsoids, thus S is a diagonal tensor – here used with two identical components:

$$S = \text{diag}(S_{g1}, S_{g1}, S_{g3}) \quad (37)$$

For air inclusions in snow the model uses spherical shapes S reducing to a scalar:

$$S = -1/(3k_0^2 K_0) \quad (38)$$

S is defined by

$$\Gamma(r, r') = S\delta(r - r') + V_P \Gamma'(r, r') \quad (39)$$

where Γ is the Green's function which allows to determine the scattering coefficients out of the ice parameters (V_P means principal value, necessary because of the strong singularity at $r = r'$). Here the tensor operator L_0^{-1} is defined by

$$L_0^{-1} = G + S. \quad (40)$$

and G is the integral operator of which kernel is $V_P \Gamma'(r, r')$. K_0 is defined by the requirement that the average of the random tensor ξ is zero:

$$\langle \xi \rangle = 0 \quad (41)$$

For the calculation of the dyadic coefficient S see Stogryn (1983b). For the case of a bounded medium with border at $z = 0$ Stogryn (1974) represents the inhomogeneity $\langle \xi G \xi \rangle \vec{E}^m$ for $z > 0$ (in air) by zero and for $z < 0$ (in snow, ice or water) by

$$\langle \xi G \xi \rangle \vec{E}^m = k_0^4 \int_{z' < 0} C(r, r') \Gamma(r, r') \vec{E}^m(r') d^3 r' \quad (42)$$

and approximates that by

$$\langle \xi G \xi \rangle \vec{E}^m = k_0^2 \kappa(z) \vec{E}^m \quad (43)$$

where

$$\kappa(z) = k_0^2 \int_{z' < 0} C(r, r') \Gamma(r, r') d^3 r'. \quad (44)$$

Here Stogryn has used the additional assumption that the correlation scale lengths of the inhomogeneities are small compared to the electromagnetic wavelength. C is a complex correlation function

$$C(r, r') = \langle (K_0 - K^r)(K_0 - K^{r'}) \rangle \quad (45)$$

of dielectric constants at different positions in space. Out of the incident field and the continuity condition of the electric field Stogryn calculates the mean field and in combination with (34) the expectation value of the product $\vec{E}^r(r) \vec{E}^{r*}(r)$. Using the calculations of Peake (1959) in Fourier space he gets the scattering coefficients:

$$\gamma_{ab}(\vec{k}_0, \vec{k}) = (4\pi \cos \theta / E_0^2 \cos \theta_0) b_i b_j \langle E_i^r(\vec{k}) E_j^{r*}(\vec{k}) \rangle \quad (46)$$

Here b_i and b_j are unit vectors. To calculate the reflection coefficients Stogryn uses boundary conditions for the mean field. The Grenfell model uses layers with constant dielectric tensors. So the integrations used for the calculations of the scattering coefficients are summations and the emissivity corresponding to polarization a in the direction $-\vec{k}_0$ is

$$\epsilon_a(\vec{k}_0) = 1 - |R_a|^2 - \frac{1}{4\pi} \int (\gamma_{ah}(\vec{k}_0, \vec{k}) + \gamma_{av}(\vec{k}_0, \vec{k})) \sin \theta d\theta d\phi. \quad (47)$$

Here is R_a the Fresnel reflection coefficient which is calculated from the mean electromagnetic field \vec{E}^m (see (49)). It describes the coherent reflection. The brightness temperature of the radiation leaving the surface $z = 0$ in the direction $-\vec{k}_0$ and with polarization a is according to Stogryn (1986)

$$TB(\vec{k}_0, 0) = \epsilon_a(\vec{k}_0) T_{ice} + |R_a|^2 TB_a + \frac{1}{4} \int (\gamma_{ah} + \gamma_{av}) TB_a(\vec{k}) \sin \theta d\theta d\phi \quad (48)$$

where T_{ice} is the thermal temperature of the sea ice (a quite well approximation seems to be the temperature of the uppermost layer). $TB_a(\vec{k})$ is the brightness temperature of the downwelling radiation incident on the sea ice surface in the direction $-\vec{k}$. The first term in (48) represents the radiation directly emitted by the sea-ice (and underlying water) while the second and third terms correspond to the specular and nonspecular scattering of the incident atmospheric radiation by the sea ice surface.

3.1.2 The Layer Structure of the Model

The ice model uses different layers for snow, ice and water to calculate the emissivity of sea ice. For snow or ice the model can use up to 20 layers. First the program calculates the dielectric tensor for every layer in the subroutine PHYS of the main program. The mean field in the sea ice is described with depth-dependent functions f for h-polarization (and

similar f_x and f_z for v-polarization). The mean field \vec{E}^m in the ice is for h-polarization

$$\vec{E}^m = \vec{h} E_0 f(z) \exp(ik \sin \theta_0 x) \quad (49)$$

with $\vec{h} = (\sin \phi, -\cos \phi, 0)^T$. The continuity of the electric field at the boundary between the air and the sea ice shows that the h-polarized reflection-coefficient is

$$R_h = f(0) - 1. \quad (50)$$

The functions f for h-polarization and f_x and f_z for v-polarization are the solutions of Riccati differential equations, see for example (Ulaby 1981). For more details see Strogryn (1987).

3.1.2.1 The sea-ice layers The model assumes sea ice as a mixture of pure ice, brine, and air. The pure ice occurs in the form of thin platelets of about 0.5 mm thick with the crystallographic axis perpendicular to the plane of the platelets. These platelets are stacked together to form grains of which average cross-sectional diameter is about 0.4 cm. The c -axis of the grains can have various orientations. For frazil (Vant 1978) and multiyear ice (Campbell 1978) of low salinity the axis may be assumed to be randomly oriented while for columnar ice there is a tendency for the polar angle of the c axis (measured from the vertical) to increase from approximately 0° near the surface to 90° as the depth increases. The azimuthal orientation of the c axis assumed random. This imposes an azimuthal symmetry on the dielectric tensor that will hold in most cases except ice formed in the presence of strongly directional currents. The brine cells in the model assumed to occur between the platelets comprising a grain and are thus perpendicular to the c axis. Structures such as brine drainage channels are included in the modeling of brine and air inclusions. Within a grain the brine cells occur as long, roughly cylindrical, parallel inclusions with random spacings. Air pockets are assumed to occur only between the ice grains. Thus, the grains consist only of brine and ice. For lack of more definitive information the air bubbles are assumed to be roughly spherical in shape so that they may be described by a spherically symmetric correlation function. In order to calculate the dielectric properties of sea ice, it is necessary to specify the dielectric constants of the constituents as well as their respective volume fractions. The brine volume will be calculated in the subroutine BRINE which uses a parametrisation of Strogryn (1987) for the temperature range below -30°C and a parametrisation of Cox and Weeks (1983) above -30°C . The calculation of the dielectric constant is described in Strogryn (1987).

The density of sea ice ranges between 0.65 and 0.92 g/cm³. The temperature of the ice is below 271 K. The salinity can vary between 0 and 100 ‰ but there is a limit depending on the temperature. If the salinity is large and the temperature of the ice is too high the equation

$$v_{ice} = 1 - v_{brine} - v_{air} \quad (51)$$